

# Clay minerals as provenance indicators in continental lacustrine sequences: the Leza Formation, early Cretaceous, Cameros Basin, northern Spain

J. ALONSO-AZCÁRATE<sup>1,\*</sup>, M. RODAS<sup>2</sup>, J. F. BARRENECHEA<sup>2</sup>  
AND J. R. MAS<sup>3</sup>

<sup>1</sup> *Facultad de Ciencias del Medio Ambiente, Fábrica de Armas, Universidad de Castilla-La Mancha, 45071 Toledo,*

<sup>2</sup> *Facultad de Ciencias Geológicas, Departamento de Cristalografía y Mineralogía, Universidad Complutense de Madrid, 28040 Madrid, and* <sup>3</sup> *Facultad de Ciencias Geológicas, Departamento de Estratigrafía, Universidad Complutense de Madrid, Instituto de Geología Económica, C.S.I.C., 28040 Madrid, Spain*

(Received 3 May 2004; revised 19 July 2004)

**ABSTRACT:** Variations in clay mineral assemblages, changes in Kübler index (KI), and the chemical composition of chlorites are used to identify source areas in the lacustrine materials in the Lower Cretaceous Leza Limestone Formation of the Cameros Basin, northern Spain. This formation has fairly homogeneous lithological characteristics and facies associations which do not allow for identification and characterization of local source areas. The Arnedillo lithosome of the Leza Limestone Formation contains a clay mineral association (Mg-chlorite, illite and smectite) indicative of its provenance. Chlorite composition and illite KI values indicate that these minerals were formed at temperatures higher than those reached by the Leza Formation which indicates its detrital origin. The similarity in the Mg-chlorite composition between the Arnedillo lithosome and the Keuper sediments of the area indicates that these materials acted as a local source area. This implies that Triassic sediments were exposed, at least locally, at the time of deposition of the Leza Formation. The presence of smectite in the Leza Formation is related to a retrograde diagenesis event that altered the Mg-chlorites in some samples.

**KEYWORDS:** provenance, lacustrine deposits, inherited Mg-chlorite, retrograde diagenesis.

Variations of provenance areas, or the participation of local source areas, within sedimentologically homogeneous successions can be difficult to determine using facies analysis and conventional stratigraphy. Variations in clay mineral assemblages and/or changes in the chemical composition of a specific clay mineral, may be useful for detecting variations in the source areas in such sedimentologically homogeneous materials (Blatt, 1985; Dilli &

Pant, 1994; Rao & Rao, 1995; Underwood and Pickering, 1996; Alonso-Azcárate *et al.*, 1997; Saleemi & Ahmed, 2000; Cavalcante *et al.*, 2003).

The aim of this paper is to explain the anomalous occurrence of a magnesian chlorite that appears locally in some clay beds within the lacustrine limestones of the Leza Formation in the Cameros Basin (Late Barremian–Early Aptian).

## GEOLOGICAL SETTING

The Cameros Basin is located on the northwestern edge of the Iberian Chain (Fig. 1) and can be

\* E-mail: jacinto.alonso@uclm.es  
DOI: 10.1180/0009855054010157

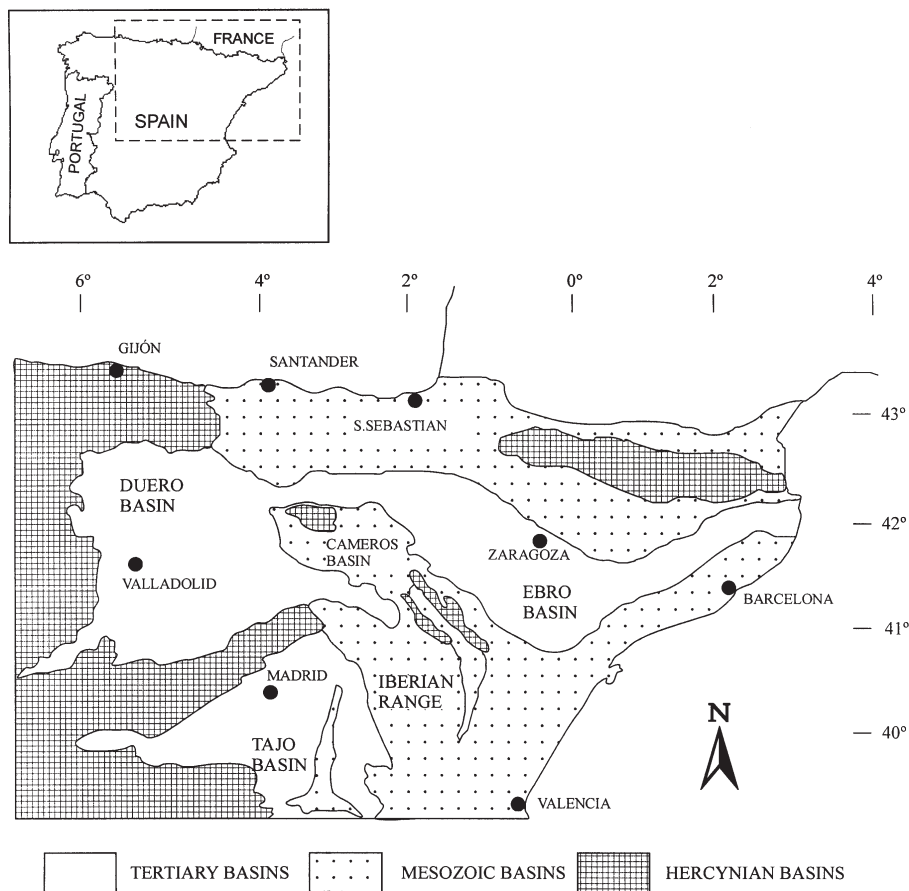


FIG. 1. Geological location of the Cameros Basin.

divided into two sub-basins, west Cameros and east Cameros; the present study deals with the east Cameros Basin. The Cameros Basin is interpreted as an extensional ramp basin (Mas *et al.*, 1993; Guimerá *et al.*, 1995).

During the Upper Jurassic–Lower Cretaceous Iberian rift, the basin had a high subsidence rate. Thus, between the Tithonian and Early Albian the sedimentary series had a vertical thickness of >5000 m (Mas *et al.*, 1993; Salas & Casas, 1993; Casas-Sainz & Gil-Imaz, 1998). The basin was formed with a palaeotopography that sloped towards the northeast. Sediment input came mainly from the southwest, from the Iberian Massif, as shown by palaeocurrent directions (Mas *et al.*, 2003).

The eastern Cameros Basin is the only basin in the Iberian Chain in which part of the sequence was affected by low-grade metamorphism. Different

studies have related this metamorphism to the circulation of hot migratory fluids within the basin (Casquet *et al.*, 1992; Barrenechea *et al.*, 1995, 2000; Alonso-Azcárate *et al.*, 1995; 1999a,b).

The infilling megasequence of the Cameros Basin can be subdivided into eight depositional sequences (Fig. 2), made up of fluviolacustrine continental materials with occasional marine sediments (Mas *et al.*, 1993). The present study deals with part of the Late Barremian–Early Aptian depositional sequence, which includes siliciclastic materials of the Urbión Group and limestones, marls and minor siliciclastic intercalations of the Enciso Group. Two formations with clearly distinct sedimentological and mineralogical characteristics within this depositional sequence can be found in the northern border of the basin: (a) the Jubera Formation, and (b) the Leza Limestone Formation. Both formations resulted from the activation of a subordinate

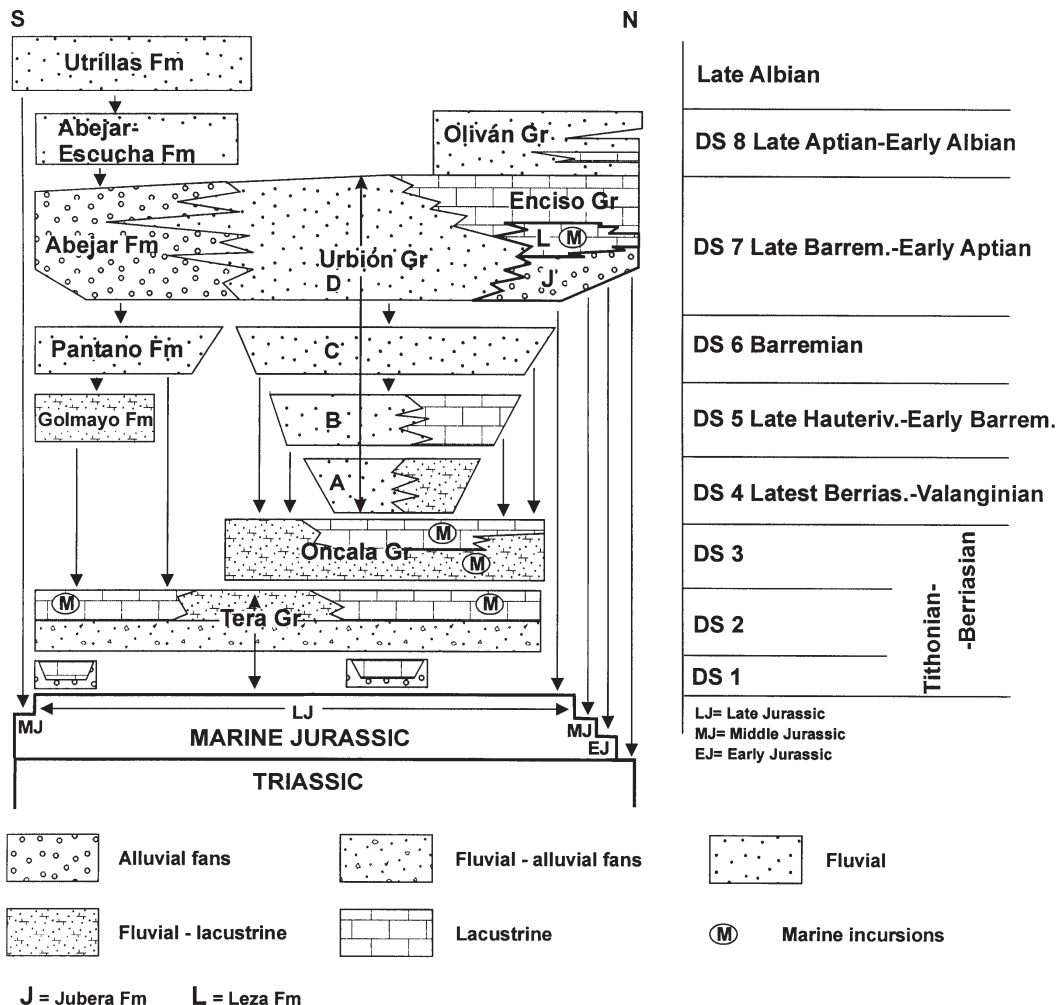


FIG. 2. Location of the Leza Formation. in the stratigraphic framework of the Cameros basin. Modified after Mas *et al.* (2003).

fracture system in this area during sedimentation (Mas *et al.*, 1993).

The Jubera Formation (Mas *et al.*, 1990), represents a lateral change of facies of the Urbión Group within depositional sequence 7 (Mas *et al.*, 1993) (Fig. 2). This unit lays unconformably on different Jurassic marine units, but very locally, towards the northwest, it rests over Triassic mudstones (Keuper facies; Alonso & Mas, 1993).

The Leza Limestone Formation (Mas *et al.*, 1990) is located stratigraphically above the Jubera Formation and changes facies laterally towards the south to the Enciso Group (Fig. 2). It consists of six carbonate lithosomes (Fig. 3) interpreted as coastal

lacustrine systems which are clearly bounded by palaeofractures (growth faults). Its genesis is controlled by syndimentary tectonics, as evidenced by abrupt facies changes and syndimentary faults recorded in sediments from the Enciso Group. The lithosomes lie along the northeast border of the basin, extend a short distance to the southwest, and have a variable thickness of 100 to 400 m (Alonso & Mas, 1993). Sediments containing small quantities of certain marine fossils (benthic foraminifers and dasycladaceae algae) interbedded with the continental lacustrine strata, are indicative of intermittent contact between the lacustrine systems and the Tethys Sea.

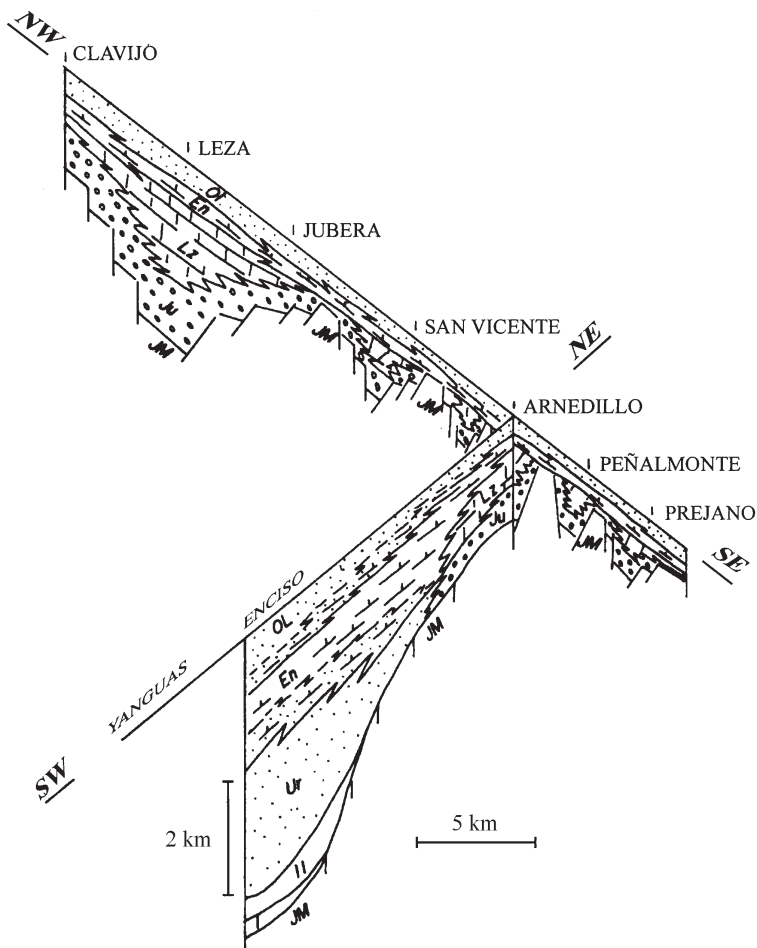


FIG. 3. Early Cretaceous correlation sections on the northeastern margin of the Cameros Basin, where the six lithosomes of the Leza Formation have been drawn. I: Tera Group, II: Oncala Group, Jm: Marine Jurassic; Ur: Urbión Group, En: Enciso Group; Ju: Jubera Formation; Lz: Leza Formation; OL: Oliván Group. Modified after Alonso & Mas (1993).

## MATERIALS AND METHODS

Three detailed stratigraphic cross-sections were recorded from the Leza Limestone Formation in the Leza, Préjano and Arnedillo lithosomes. The sections are 202 m, 93 m and 218 m thick, respectively, and are made up predominantly of limestones and sandstones. Every lutitic and marly interval from the three sections was sampled for mineralogical analysis (11 from Arnedillo, six from Prejano and six from Leza). Lutitic sediments from the Keuper facies around the Arnedillo section were also sampled (10 samples).

After grinding and homogenization of the samples to  $<53 \mu\text{m}$ , non-oriented powders were examined on a Philips PW 1730/90 diffractometer, using  $\text{Cu-K}\alpha$  radiation, graphite monochromator, ratemeter  $1 \times 10^3$  cps at time constant 1, tube power of 40 kV, 40 mA and a scan rate of  $2^\circ/2\theta/\text{min}$ . Oriented aggregates of the  $<2 \mu\text{m}$  fraction were obtained by sedimentation from an aqueous suspension onto glass slides, and were subjected to thermal treatment at  $550^\circ\text{C}$  for 2 h and to solvation with ethylene glycol (EG).

The presence of kaolinite, which can be hidden by the chlorite reflections, was checked by the

absence of the kaolinite  $d_{002}$  reflection at 3.57 Å which is easily differentiated from the chlorite  $d_{003}$  reflection at 3.51 Å (Moore & Reynolds, 1997). Semi-quantitative analysis was made following Schultz's (1964) method.

In order to determine the intensity of the post-sedimentary processes that affected these samples, the full-width-half-maximum (FWHM) of the illite 10 Å reflection (the so-called Kübler index, KI), was measured on the XRD patterns of the <2 µm material. Our data ( $y$ ) were transformed to CIS data ( $x$ ) (Warr & Rice, 1994) by the formula:  $y = 0.869x + 0.0022$ . Therefore, KI values quoted in the following parts of this study have been converted to the Kübler scale (Kübler, 1967, 1968) in which the anchizone limit values are 0.25–0.42°Δ2θ.

A petrographic microscope was used for the study of thin sections to select optimal areas for high resolution transmission electron microscopy (HRTEM) and analytical electron microscopy (AEM). Two different sample preparation methods were followed: (1) thin sections were glued onto Cu grids with a single central hole of 200–400 µm in diameter and thinned by an argon ion mill (Gatan Dual Ion Milling 600). Two ion-milling conditions were used: (a) 6 kV, 1 A and 15° incident angle while perforating; (b) 6 kV, low-angle (12°) and low-current (0.4 A) final milling for approximately 4 h to clean the sample surface. (2) The samples were crushed gently in an ethanol-filled mortar to suspend the clay. Particles were deposited onto a lacy C-coated Cu grid. The clay particles obtained were thus aligned with (00l) planes approximately perpendicular to the electron beam ( $c^*$  parallel to beam).

Samples were analysed at Granada University with a Philips CM20, AEM operating at 200 kV, with a LaB<sub>6</sub> filament, and a point-to-point resolution of 2.7 Å. Analytical electron microscopy (AEM) was performed near crystallite edges in the Cu-grid grain mounts or from individual crystallite packets in ion-milled samples. Diffraction patterns were obtained from selected areas (SAED) in regions composed of a packet of layers attributed to a single crystallite. The microscope was equipped with an X-ray energy dispersive (EDS) EDAX DX 4 spectrometer which allowed quantitative analyses of areas with a minimum size of 200 × 1000 Å.

Electron microprobe analyses (EMPA) of chlorite were performed using wavelength-dispersive spectroscopy (WDS) on a JEOL JXA-8900M at Complutense University. Operating conditions included an accelerating voltage of 15 kV, a beam

current of 20 nA and a beam diameter of 2–5 µm. The EMPA analyses were performed on detrital chlorite grains with long axes ranging from 30 to 120 µm. The standards used are described by Jarosevich *et al.* (1980) and were provided by the Smithsonian Institution, Washington D.C. Chlorite structural formulae were calculated based on a total negative charge of 28 and all Fe was taken as Fe<sup>2+</sup>. Smectite and illite structural formulae were calculated based on a total negative charge of 22 and all Fe was taken as Fe<sup>3+</sup>.

## RESULTS

### *X-ray diffraction (XRD)*

The bulk mineralogy of the three stratigraphic sections studied comprises carbonates (calcite and dolomite), alkali feldspars, quartz and phyllosilicates (Table 1). The clay mineralogy varies significantly depending on the stratigraphic section studied.

Illite is the dominant clay mineral in the Leza and Préjano sections. Small amounts of irregular chlorite-vermiculite mixed-layers and ferrous chlorite are also found in the Leza and Préjano sections respectively (Table 1). This composition is similar to that recorded for the Enciso Group in other areas (Alonso-Azcárate *et al.*, 1995, 1999c; Alonso-Azcárate, 1997; Mata *et al.*, 2001).

The mineralogy of the Arnedillo section is clearly different (Table 1). At the base of the section the relative proportion of phyllosilicates is low and chlorite appears as the principal clay mineral. Chlorite reflections in XRD patterns show very intense odd order 00l reflections, indicating that the chlorite is Mg-rich. The petrographic study reveals the occurrence of large flakes of chlorite ( $\approx 90 \times 20$  µm) in these samples. Illite and smectite occur in very small to trace amounts. Towards the top of the section, the relative proportion of phyllosilicates is much higher (Table 1). Illite becomes the dominant clay mineral, with minor amounts of chlorite and smectite. The presence of higher-order diffraction peaks at  $\sim 8.5$  Å in the glycol-solvated samples and the absence of reflections between  $\approx 10$  and 17 Å or at  $>17$  Å, indicate that smectite does not contain mixed layers of other phyllosilicates (Reynolds, 1980; Moore & Reynolds, 1997).

Figure 4 shows a histogram of the Kübler index for the samples from the Leza Formation in the

TABLE 1. Mineralogical composition of the Leza Formation.

Lithosome	Samples	Dist (m)	Bulk mineralogy (%)					Clay mineralogy (%)			
			Cal	Dol	Fto	Q	Phy	Chl	Ill	Sm	ML
Arnedillo section	ARN-11-	212	33	14	T	5	46	15	77	8	—
	ARN-10-	183	52	7	—	5	36	24	43	33	—
	ARN-9-	152	—	—	T	5	95	—	87	13	—
	ARN-8-	71	5	—	5	9	81	T	66	34	—
	ARN-7-	62	—	—	10	5	85	T	100	—	—
	ARN-6-	56	—	12	7	5	76	52	48	—	—
	ARN-5-	32	71	—	8	5	16	88	12	T	—
	ARN-4-	21	78	—	6	9	7	100	T	—	—
	ARN-3-	15	54	12	8	7	19	100	T	—	—
	ARN-2-	11	41	—	5	5	49	89	T	11	—
Prejano section	ARN-1-	6	43	57	—	T	T	100	T	T	—
	PRE-7-	90	—	—	9	7	84	T	10	—	—
	PRE-6-	65	23	—	5	5	67	T	100	—	—
	PRE-5-	53	33	20	T	5	42	20	80	—	—
	PRE-4-	42	23	—	5	5	67	9	91	—	—
	PRE-3-	23	10	—	7	6	77	T	100	—	—
	PRE-2-	17	5	—	13	8	74	—	100	—	—
Leza section	PRE-1-	5	23	—	—	5	72	—	100	—	—
	LEZ-6-	176	67	—	—	5	28	—	10	—	—
	LEZ-5-	164	50	—	—	5	45	—	100	—	T
	LEZ-4-	158	90	—	—	10	T	—	100	—	—
	LEZ-3-	125	94	—	—	6	T	—	100	—	T
	LEZ-2-	81	5	—	—	5	90	—	100	—	T
	LEZ-1-	63	—	—	5	9	86	—	100	—	T

Dist: distance to the base of the section, Cal: calcite, Dol: dolomite, Fto: feldspar, Q: quartz, Phy: phyllosilicates, Chl: chlorite, Ill: illite, Sm: smectite, ML: irregular mixed-layer, T: trace amounts.

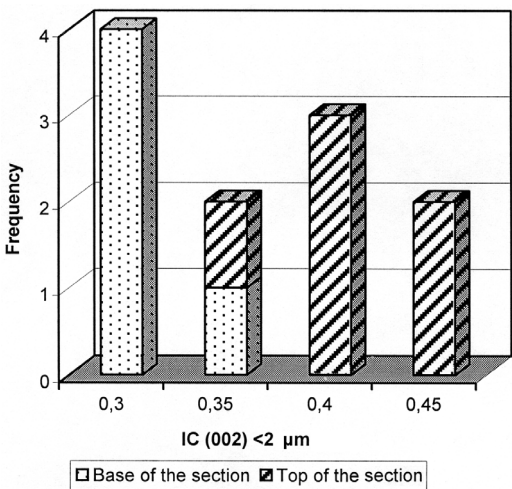


FIG. 4. Kübler index data for the Arnedillo stratigraphic section.

Arnedillo section. Here, the FWHM has smaller values (higher crystallinities) for the chlorite-rich samples with an average value of  $0.27^{\circ}\Delta 2\theta$ , while the illites from the top of the series have an average value of  $0.37^{\circ}\Delta 2\theta$ . Both values indicate high-anchizone conditions, which clearly contrast with the diagenetic conditions close to the anchizone boundary (mean value of  $0.46^{\circ}\Delta 2\theta$ ) recorded by Alonso-Azcárate *et al.* (1999c) for the overlying Enciso Group.

HRTEM and compositional data

Four samples (ARN 2, 3, 8 and 10) representative of the Leza Formation in the Arnedillo cross-section and three samples from the Keuper facies cropping out in the area were chosen for the HRTEM-AEM study. Based on lattice-fringe images and SAED patterns, three different phyllosilicates can be distinguished: chlorite, smectite and



illite. Representative AEM and EMPA data of these phases are presented in Table 2.

Chlorite from the Leza Formation in the Arnedillo section can be found as large (30–120  $\mu\text{m}$ ) elongated grains and as fine-grained particles within the clayey matrix. When observed by HRTEM they show lattice-fringe images with uniform contrast and undeformed straight defect-

free 14 Å layers (Fig. 5a). The mineral comprises aggregates of subparallel packets of layers that display lattice fringes over relatively large areas. The thickness of individual chlorite packets varies from 100 to 3000 Å, with a mean value of ~300 Å. They show no layer terminations and few low-angle boundaries. A semi-random stacking polytype is frequently found (Fig. 6a) although in places the

TABLE 2. Selected AEM and EMPA analyses in atoms per formula (a.p.f.u.).

	Si	<sup>IV</sup> Al	<sup>VI</sup> Al	Fe <sup>2+</sup>	Fe <sup>3+</sup>	Mg	Ca	K	Na	$\Sigma_{\text{oct}}$
Chlorites from the Arnedillo section										
Pure chlorites	2.99	1.01	1.01	0.7	—	4.21	—	—	—	6.00
	3.02	0.98	0.97	0.75	—	4.29	—	—	—	6.01
	2.92	1.08	0.78	0.77	—	4.60	—	—	—	6.15
	2.95	1.05	0.95	0.87	—	4.23	—	—	—	6.05
Altered chlorites	3.22	0.78	1.43	0.67	—	3.05	0.41	0.2	—	5.14
	3.20	0.80	1.14	0.67	—	4.03	0.27	—	—	5.84
	3.36	0.64	1.40	0.02	—	4.05	0.20	0.10	—	5.47
	3.18	0.82	1.21	0.02	—	4.57	0.22	—	—	5.80
Chlorite grains	2.96	1.04	1.07	0.58	—	4.33	—	0.03	—	5.98
	2.92	1.08	1.05	0.50	—	4.47	—	—	—	6.02
	3.25	0.75	1.22	0.73	—	3.80	0.10	0.11	—	5.76
	3.39	0.61	1.55	0.38	—	3.60	0.08	0.07	—	5.53
PRE										
	2.93	1.07	1.70	2.34	—	1.65	—	0.2	—	5.69
	3.04	0.96	1.28	3.45	—	0.82	—	0.5	—	5.55
M										
	2.57	1.43	1.68	2.94	—	1.13	0.1	0.25	—	5.75
	2.94	1.07	1.76	1.38	—	2.44	—	0.31	—	5.58
Chlorites from the Keuper facies										
	3.07	0.93	1.25	0.62	—	3.95	0.01	0.01	—	5.82
	3.07	0.93	1.15	0.63	—	4.10	0.05	0.07	—	5.88
	3.09	0.91	1.29	0.76	—	3.71	0.02	0.06	—	5.76
	3.17	0.83	1.11	0.81	—	3.87	0.03	0.03	—	5.79
Smectites from the Arnedillo section										
	3.39	0.61	1.54	—	0.15	0.56	0.18	0.07	—	2.25
	3.68	0.32	1.55	—	0.02	0.64	—	0.35	—	2.20
	3.72	0.28	1.73	—	0.01	0.36	—	0.36	—	2.10
	3.84	0.16	1.57	—	0.01	0.47	0.24	—	—	2.05
	3.53	0.47	1.82	—	0.01	0.26	0.21	0.05	—	2.09
Illites from the Arnedillo section										
	3.10	0.90	1.51	—	0.21	0.26	—	0.90	0.10	1.98
	3.02	0.98	1.29	—	0.21	0.72	—	0.75	—	2.22
	2.98	1.02	1.85	—	0.06	0.14	—	0.54	0.32	2.05
	3.26	0.74	1.67	—	0.02	0.38	—	0.92	—	2.07

PRE: chlorites from Préjano section. M: composition of two typical chlorites from the Enciso Group.

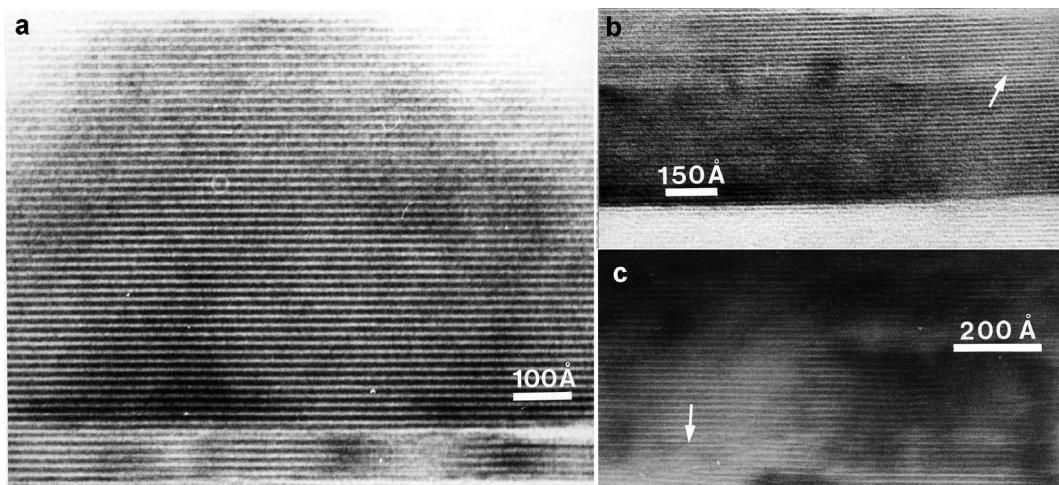


FIG. 5. Lattice-fringe images showing portions of chlorite grains: (a) consisting of straight 14 Å fringes; (b) with an individual interstratified 10 Å layer (white arrow); (c) showing a 14 to 10 Å lateral transformation (white arrow).

ordered one-layer polytype is found. Both the AEM analysis on finely grained chlorite from the matrix (pure chlorites, Table 2) and the EMPA data from some of the larger chlorite grains (chlorite grains, Table 2), reveal high Mg contents,  $^{IV}Al/^{VI}Al$  ratios close to 1 and octahedral occupancies close to the ideal value for a trioctahedral chlorite.

Individual 10 Å layers are sometimes observed within chlorite packets (Fig. 5b). Occasionally 10 Å fringes change along-layer to 14 Å fringes (Fig. 5c). SAED patterns also show the presence of both tri- and dioctahedral phyllosilicates (Fig. 6d). The AEM analyses in these areas show significant proportions of Ca and minor K, together with high Si and  $^{VI}Al$  contents in the chlorite formulae (altered chlorites, Table 2). These compositional features suggest that the 10 Å layers interstratified with chlorite are smectite layers. The small proportions of K+Ca together with lower octahedral total occupancy in some chlorite grains analysed by EMPA (chlorite grains, Table 2) also point to the presence of smectite layers interstratified with the chlorite. Although apparently pure under the petrographic microscope and the microprobe optical system, the low optical resolution of these techniques, compared to TEM precludes the possibility of detecting scattered layers of other phyllosilicates interstratified with the chlorite.

Chlorite from the Keuper facies displays lattice-fringe images with features like those observed in

samples from the Leza Formation in the Arnedillo section. The range of chemical compositions determined by AEM is also very similar (Table 2). All the chlorites analysed in this study by AEM and EMPA plot within an elongated area in the Si- $Al_{tot}$ -Fe+Mg diagram (Fig. 7), close to the Fe+Mg corner. However, analyses from areas where 10 Å layers are intergrown within chlorite packets plot at intermediate positions between chlorite and smectite end-member compositions. The data of all the chlorites have been also represented in a Si-Mg-Fe ternary diagram (Fig. 8) and they all plot close to the composition of pure clinocllore (Wiewiora & Weiss, 1990), indicating that there is only one sample population.

Illite and smectite both give lattice-fringe spacings of  $\sim 10$  Å because the hydrated smectite layers, with an approximate thickness of 14 Å, collapse to 10 Å in the high vacuum of the TEM. Nevertheless, they are easily distinguished by several features. On one hand, illite occurs as straight lattice-fringe packets up to 800 Å thick. Images of the mineral show a strong mottled structure, no layer terminations and  $2M$  polytype. On the other hand, smectite packets are thin with slightly wavy lattice fringes, poor contrast and have frequent layer terminations. Smectite is associated with chlorite packets coherently intergrown with parallel (001) planes. Lattice fringe images for smectite are difficult to obtain because layers are easily damaged by the electron beam. Smectite



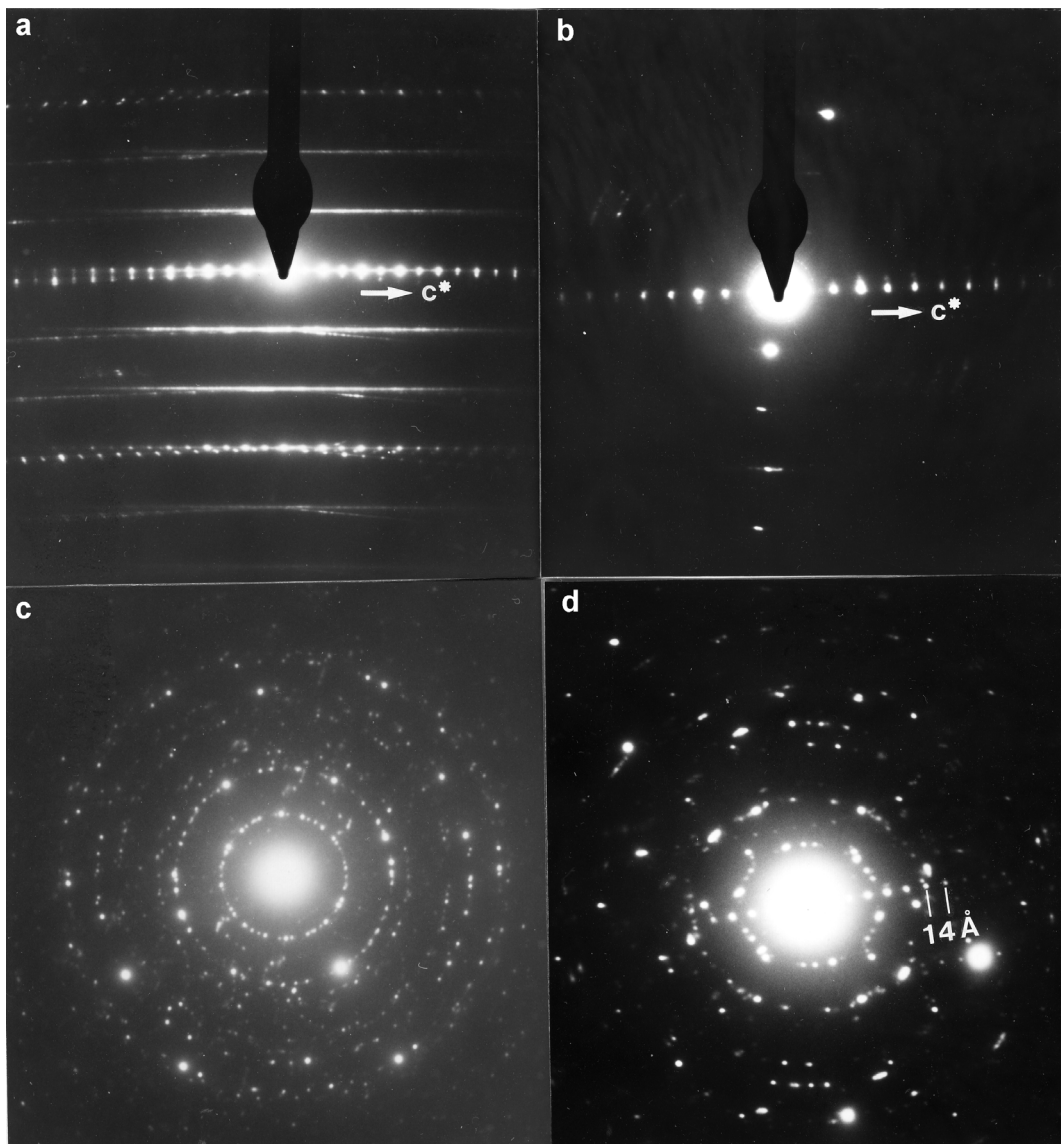


FIG. 6. SAED patterns of: (a) chlorite semi-random stacking polytype; (b) smectite; (c) smectite showing rings of spots reflecting polycrystalline diffractions of multiple small crystals stacked in different directions; and (d) intergrown smectite (rings) and chlorite ( $14 \text{ \AA}$  reflections).

SAED patterns are diffuse and elongated in a direction normal to  $c^*$  (Fig. 6b); they frequently show rings of spots which reflect polycrystalline diffractions of multiple small crystals stacked in different directions (Fig. 6c). Smectite and illite are also readily distinguished by AEM analyses. Al-rich dioctahedral smectites with minor Mg and a composition close to the beidellite end-member

(Moore & Reynolds, 1997) have been recognized (Table 2). Smectite shows a higher Si content than illite and the interlayer cation position is occupied by either K or Ca, or both.

Representative analyses of illite are included in Table 2. The interlayer space has a high occupancy, close to the muscovite end-member. The main cation is K, although small amounts of Na are also

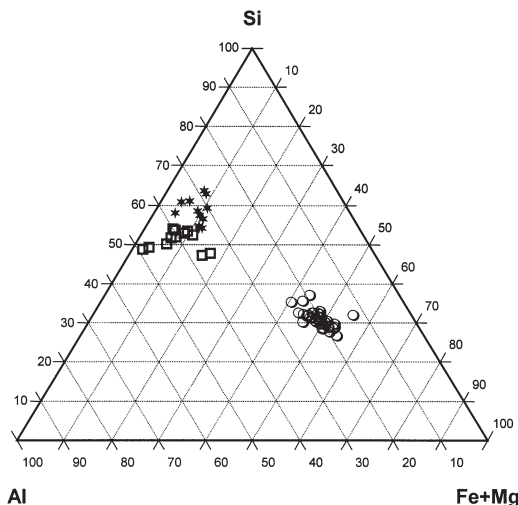


FIG. 7. Si-Al<sub>tot</sub>-Fe+Mg triangular plot (atoms per formula unit) of the chemical composition data for phyllosilicates in the Arnedillo area. ○: chlorite; □: illite; ★: smectite.

found in some crystals. Differentiation of illite layers as opposed to smectite layers was determined by the higher illite K content in the AEM analyses.

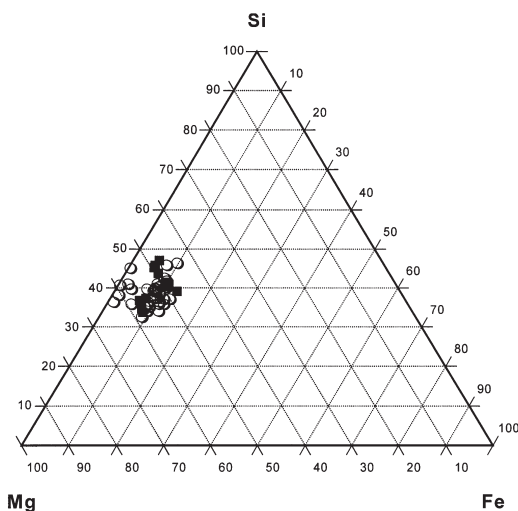


FIG. 8. Si-Mg-Fe triangular plot (atoms per formula unit) of the chemical composition data for chlorites in the Arnedillo area. ○: chlorites from the Leza Formation in the Arnedillo section; ■: chlorites from the Keuper facies around the Arnedillo stratigraphic section.

## DISCUSSION

The mineralogical composition of the Leza Formation in the Arnedillo section contrasts with the composition of the materials found in the rest of the Leza Formation and Enciso Group. According to Alonso-Azcárate (1997) and Alonso-Azcárate *et al.* (1999c), the sediments in the Arnedillo area reached metamorphic conditions close to the diagenesis-anchizone boundary. However, Kübler index data presented in this study for the Leza Formation (Fig. 4) fall within the anchizone-epizone limit. Thus illite in these samples appears to have been formed under metamorphic conditions that were higher than in the rest of the Leza Formation and the Enciso Group.

In addition, the Mg-rich composition of the chlorites in the Arnedillo section differs from the average composition of chlorites from the Leza Formation, the Enciso Group and the rest of lacustrine sediments of the basin (Fig. 9). They have a very high Mg content with a composition close to the clinocllore end-member (Table 2). No K or Ca is present in the pure chlorites. K and Ca detected in some chlorite analyses are attributed to a small proportion of smectite layers interstratified at a fine scale, as shown by the TEM images (Fig. 5b). The proportion of <sup>IV</sup>Al and <sup>VI</sup>Al of the

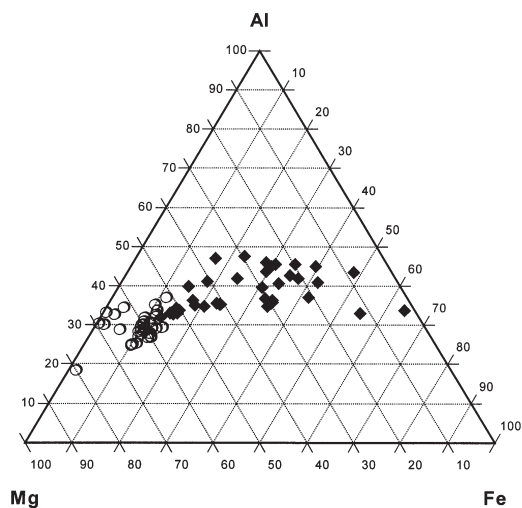


FIG. 9. Al-Mg-Fe triangular plot (atoms per formula unit) of all the chlorites in the lacustrine formations of the Cameros basin. ○: chlorites from the Leza Formation in the Arnedillo section; ◆: chlorites from the Leza Formation, the Enciso Group and the rest of lacustrine sediments of the basin.

pure chlorites is very similar ( $^{IV}Al/^{VI}Al$  ratios close to 1), while the rest of the chlorites analysed show lower  $^{IV}Al/^{VI}Al$  ratios (Table 2). Pure chlorites have nearly ideal octahedral occupancy. These characteristics are typical of metamorphic chlorites that have been subjected to higher temperatures (Hillier & Velde, 1991) than those reached by this unit. Therefore, the clay mineralogy (illite and chlorite) in the samples from the Arnedillo section seems to have an origin inherited from source areas which have experienced more severe metamorphic conditions.

### *Provenance of the chlorite*

The palaeocurrents measured in the Jubera Formation show that detritus was derived from the north (Mas *et al.*, 2003). The Leza Formation is the upper part of a carbonate-siliciclastic cycle (Jubera and Leza Formations) that reflects a decrease in tectonic activity at the northern edge of the basin during sedimentation. Therefore, during deposition of these formations, terrigenous materials were derived from source areas located to the north of the basin. These comprise mainly Mesozoic strata (essentially Jurassic), as shown by the clast composition of the Jubera Formation conglomerates (Alonso & Mas, 1993). The chemical composition of the chlorites from the Leza Formation and those from the Keuper sediments (Table 2, Figs 7,8) represent a single population. Considering the high variability that chlorite composition can exhibit (Wiewiora & Weiss, 1990; Zane *et al.*, 1998) and the unusual composition of these two groups of samples, these chlorites appear to have a common origin. Therefore, the most probable origin for the Mg-chlorites of the Leza Formation is that they were inherited from the Triassic sediments, which implies that at the time of deposition of the Leza Formation, Triassic sediments were exposed, at least locally. This is an important conclusion as the presence of this provenance area cannot be deduced solely from sedimentary and/or stratigraphic criteria.

During deposition of the Leza Formation, the source areas moved progressively from the northern border to the southwestern border of the basin (Alonso & Mas, 1993; Mas *et al.*, 2003). This was probably due to the decreasing tectonic activity along the faults bounding the northern edge of the basin that controlled sedimentation. The new input of materials from the southern border had a

significant effect on the clay mineralogy of the sediments. Towards the top of the section an increase in the clay mineral content is produced and illite is the main phyllosilicate in the clay fraction (Table 1), as is usual in the Enciso Group. The increase in the KI values measured in the top of the section, with intermediate values between the base of the section and the overlying Enciso Group suggest that the detrital supply from the northern sector decreased, with the southwest sector becoming the main source area; although some input from the northern border is still present as suggested by the presence of Mg-chlorite. The absence of Mg-rich chlorites in the rest of the carbonate lithosomes studied in the Leza Formation seems to indicate the presence of different local source areas for each lithosome.

An alternative hypothesis is that marine or lacustrine waters rich in Mg led to the formation of chlorite. The formation of magnesium rather than iron chlorites is favoured in marine (Lucas and Ataman, 1968) and lacustrine-evaporitic environments (Hillier, 1993; Alonso-Azcárate, 1997; Barrenechea *et al.*, 2000). However, the singularity of the chlorite composition in the context of the basin (Barrenechea *et al.*, 1995; Alonso-Azcárate, 1997; Barrenechea *et al.*, 2000) and the perfect match with the compositional features of the chlorite from the Keuper facies support an inherited origin (Fig. 8).

### *Formation of retrograde smectite*

The occurrence of smectite in the sediments is incompatible with the metamorphic grade reached by these materials. Smectite is unstable at temperatures exceeding 200°C (Essene & Peacor, 1995) and at lower temperatures smectite starts to evolve to chlorite (Bodine & Madsen, 1987) or illite (Hillier & Clayton, 1989; Šucha *et al.*, 1993) depending on the chemistry of the environment and the smectite composition. This temperature range was exceeded by these sediments according to the estimations of the metamorphic degree of the area based on illite and chlorite crystallinities (Alonso-Azcárate *et al.*, 1999c). The most likely origin for the smectite is the alteration of Mg-rich chlorites during “retrograde diagenesis”, as defined by Nieto *et al.* (1994). In fact, as seen in TEM images, the smectites are always associated with Mg-chlorites. In samples from the base of the section, where there is a small proportion of smectite in the clay

fraction, the alteration process is minimal and could be in an early stage. These are the only samples where individual 10 Å smectite layers frequently appear interlayered in the chlorite packets. In samples from the top of the section, the alteration reaction has progressed further so that small packets of smectite are coherently intergrown with chlorite packets. SAED patterns reflect interlayering of chlorite and smectite packets (Fig 6d).

The replacement of a trioctahedral Mg-rich mineral by a dioctahedral Al-rich mineral might seem unusual, especially when dioctahedral illite is present in the samples. Nieto *et al.* (1994) pointed out that the key factor in this type of alteration is the difference in composition between the post-peak metamorphic fluids producing the alteration process and the chlorite. The reaction requires the introduction of Si, Ca and K and loss of Mg. Retrograde reactions involve dissolution and crystallization through hydration, thus water must play a significant role, since solid-state reactions are negligible at low temperature (Zhao *et al.*, 1999). During the development of the metamorphism the fluid/rock ratio was very high as shown by pyrite mineralization in the area (Alonso-Azcárate *et al.*, 1999a) and by the distribution of mineral associations (Alonso-Azcárate *et al.*, 1995; Barrenechea *et al.*, 1995, 2000). However, with the data available we cannot determine the exact timing of the retrograde alteration process.

## CONCLUSIONS

The compositional features in the fine fraction of the lutitic and marly samples of the Leza Formation (Late Barremian–Early Aptian) in the Arnedillo section are substantially different from the rest of the series in the Formation and from the materials of the Enciso Group.

Mg-chlorite (characterized by  $^{IV}Al/^{VI}Al$  ratios >1 and the absence of octahedral vacancies and K-Ca) is the main phyllosilicate, with minor amounts of illite and smectite, while in the rest of the series the clay fraction is composed of illite and Fe-rich chlorite. The Kübler index in these sediments reflects higher-grade metamorphic conditions (limit anchizone-epizone) than those of the area in which it is found (diagenesis).

Therefore, the fine fraction of this series seems to have an origin inherited from source areas with materials which had reached higher-grade metamorphic conditions than those to which the

sediments were later subjected. Since the composition of chlorite for the Leza Formation matches that of the Keuper facies, a source area on the Keuper sediments can be deduced. This implies that the Keuper sediments were exposed, at least locally, at the time of the basin infilling. The presence of smectite is related to a 'retrograde diagenesis' process that involved the alteration of Mg-chlorite to smectite.

Based on mineralogical data, we infer the presence of local source areas for these sediments which are different from those in the rest of the sequence. These sources would have been difficult to detect with sedimentological or stratigraphic information alone, due to the homogeneity of the materials present in the Leza Limestone Formation.

## ACKNOWLEDGMENTS

We wish to thank Dr Juan Carlos Fernandez Caliani for valuable discussions of an early version of the manuscript and José Luis González Pachón for the photographic work. This work was supported by the research project PB94-0054 from DGICYT (Dirección General de Investigación Científica y Técnica). Maria del Mar Abad is thanked for assistance with the TEM analytical work. We are grateful to Prof. Fernando Nieto for his extensive help during the development of this work.

## REFERENCES

- Alonso A. & Mas J.R. (1993) Control tectónico e influencia del eustatismo en la sedimentación del Cretácico inferior de la Cuenca de Los Cameros. España. *Cuadernos de Geología Ibérica*, **17**, 285–310.
- Alonso-Azcárate J. (1997) *Evolución de los filosilicatos y génesis de los yacimientos de piritita en la cuenca de Cameros: su relación con las facies sedimentarias y el metamorfismo*. PhD thesis, Universidad Complutense de Madrid, Spain, 544 pp.
- Alonso-Azcárate J., Barrenechea J.F., Rodas M. & Mas J.R. (1995) Comparative study of the transition between very low-grade and low-grade metamorphism in siliciclastic and carbonate sediments: Early Cretaceous, Cameros Basin (Northern Spain). *Clay Minerals*, **30**, 407–419.
- Alonso-Azcárate J., Arche A., Barrenechea J.F., López-Gómez J., Luque F.J. & Rodas M. (1997) Palaeogeographical significance of clay mineral assemblages in the Permian and Triassic sediments of the SE Iberian Ranges, eastern Spain. *Palaeogeography, Palaeoclimatology,*



- Palaeoecology*, **136**, 309–330.
- Alonso-Azcárate J., Rodas M., Bottrell S.H., Raiswell R., Velasco F. & Mas J.R. (1999a) The pyrite deposits of the Cameros Basin, Spain: evidence for channelling of peak metamorphic fluid flow through sandstone aquifers. *Journal of Metamorphic Geology*, **17**, 339–348.
- Alonso-Azcárate J., Boyce A.J., Bottrell S.H., Macaulay C.I., Rodas M., Fallick A.E. & Mas J.R. (1999b) Development and use of in situ laser sulfur isotope analyses for pyrite-anhydrite geothermometry: An example from the pyrite deposits of the Cameros Basin, NE Spain. *Geochimica et Cosmochimica Acta*, **63**, 509–513.
- Alonso-Azcárate J., Rodas M., Barrenechea J.F. & Mas J.R. (1999c) Factores que controlan la evolución de los parámetros cristaloquímicos y asociaciones minerales en las rocas sedimentarias del grupo Enciso (Cretácico inferior). Cuenca de Cameros, La Rioja (norte de España). *Revista de la Sociedad Geológica de España*, **12**, 439–451.
- Barrenechea J.F., Rodas M. & Mas J.R. (1995) Clay mineral variation associated with diagenesis and low-grade metamorphism of Early Cretaceous sediments in the Cameros basin, Spain. *Clay Minerals*, **30**, 119–133.
- Barrenechea J.F., Rodas M., Frey M., Alonso-Azcárate J. & Mas J.R. (2000) Chlorite, corrensites, and chlorite-mica in late Jurassic fluvio-lacustrine sediments of the Cameros basin of northeastern Spain. *Clays and Clay Minerals*, **48**, 256–265.
- Blatt H. (1985) Provenance studies and mudrocks. *Journal of Sedimentary Petrology*, **55**, 69–75.
- Bodine M.W. Jr. & Madsen B.M. (1987) Mixed-layer chlorite/smectites from a Pennsylvanian evaporite cycle, Grand County, Utah. Pp. 85–93 in: *Proceedings of the International Clay Conference*, vol. 8. The Clay Minerals Society, Boulder, Colorado.
- Casas-Sainz A.M. & Gil-Imaz A. (1998) Extensional subsidence, contractional folding and thrust inversion of the Eastern Cameros Massif, northern Spain. *Geologische Rundschau*, **86**, 802–818.
- Casquet C., Galindo C., González Casado J.M., Alonso A., Mas R., Rodas M., García E. & Barrenechea J.F. (1992) El metamorfismo en la Cuenca de los Cameros. Geocronología e implicaciones tectónicas. *Geogaceta*, **11**, 22–25.
- Cavalcante F., Fiore S., Piccarreta G. & Tateo F. (2003) Geochemical and mineralogical approaches to assessing provenance and deposition of shales; a case study. *Clay Minerals*, **38**, 383–397.
- Dilli K. & Pant R.K. (1994) Clay minerals as indicators of the provenance and palaeoclimatic record of the Kashmir Loess. *Journal of the Geological Society of India*, **44**, 563–574.
- Essene E.J. & Peacor D.R. (1995) Clay mineral thermometry – a critical perspective. *Clays and Clay Minerals*, **43**, 540–553.
- Guimerá J., Alonso A. & Mas J. R. (1995) Inversion of an extensional-ramp basin by a newly formed thrust: the Cameros basin (N. Spain). Pp. 433–453 in: *Basin Inversion* (J.C. Buchanan and P. Buchanan, editors). Special Publication, **88**. Geological Society of London.
- Hillier S. (1993) Origin, diagenesis and mineralogy of chlorite minerals in Devonian lacustrine mudrocks, Orcadian Basin, Scotland. *Clays and Clay Minerals*, **41**, 240–259.
- Hillier S. & Clayton T. (1989) Illite/smectite diagenesis in Devonian lacustrine mudrocks from northern Scotland and its relationship to organic maturity indicators. *Clay Minerals*, **24**, 181–196.
- Hillier S. & Velde B. (1991) Octahedral occupancy and the chemical composition of diagenetic (low-temperature) chlorites. *Clay Minerals*, **26**, 149–168.
- Jarosewich E., Nelen J.A. & Norberg A. (1980) Reference samples for electron microprobe analysis. *Geostandards Newsletter*, **4**, 43–47.
- Kübler B. (1967) La cristallinité de l'illite et les zones tout à fait supérieures du métamorphisme. *Etages Tectoniques. Coll Neuchâtel*, 105–122.
- Kübler B. (1968) Evaluation quantitative du métamorphisme par la cristallinité de l'illite. *Bulletin de Centre Recherche, Pau SNPA*, **2**, 385–397.
- Lucas J. & Ataman G. (1968) Mineralogical and geochemical study of clay mineral transformations in the sedimentary Triassic Jura basin (France). *Clays and Clay Minerals*, **16**, 365–372.
- Mas J.R., Alonso A. & Díaz E. (1990) Tectonically controlled carbonate lacustrine systems in the northern margin of the Cameros Basin (Lower Cretaceous, North Spain). P. 55 in: *6th Meeting of the European Geological Societies*, Lisbon.
- Mas J.R., Alonso A. & Guimerá J. (1993) Evolución tectonosedimentaria de una cuenca extensional intraplaca: la cuenca finijurásica-eocretácica de Los Cameros (La Rioja-Soria). *Revista de la Sociedad Geológica de España*, **6**, 129–144.
- Mas J.R., Benito M.I., Arribas J., Serrano A., Guimerá J., Alonso A. & Alonso-Azcárate, J. (2003) The Cameros Basin: From Late Jurassic-Early Cretaceous Extension to Tertiary Contractional Inversion-Implications of Hydrocarbon Exploration. Northwest Iberian Chain, North Spain. P. 56 in: *Geological Field Trip 11. AAPG International Conference and Exhibition*; Barcelona, Spain. Centre Recherches, Elf-Total-Fina.
- Mata M.P., Casas A.M., Canals A., Gil A. & Pocovi A. (2001) Thermal history during Mesozoic extension and Tertiary uplift in the Cameros Basin, northern Spain. *Basin Research*, **13**, 91–111.
- Moore D.M. & Reynolds R.C. Jr. (1997) *X-ray Diffraction and the Identification and Analysis of*



- Clay Minerals*, 2<sup>nd</sup> edition, p. 332. Oxford University Press, New York.
- Nieto F., Velilla N., Peacor D.R. & Ortega Huertas M. (1994) Regional retrograde alteration of sub-greenschist facies chlorite to smectite. *Contributions to Mineralogy and Petrology*, **115**, 243–252.
- Rao V.P. & Rao B.R. (1995) Provenance and distribution of clay minerals in the sediments of the western continental shelf and slope of India. *Continental Shelf Research*, **15**, 1757–1771.
- Reynolds R.C. Jr. (1980) Interstratified clay minerals. Pp. 335–380 in: *Crystal Structures of Clay Minerals and their X-ray Identification* (G.W. Brindley and G. Brown, editors). Monograph **5**, Mineralogical Society, London.
- Salas R. & Casas A. (1993) Mesozoic extensional tectonics, stratigraphy and crustal evolution during the Alpine cycle of the eastern Iberian basin. *Tectonophysics*, **228**, 33–35.
- Saleemi A.A. & Ahmed Z. (2000) Mineral and chemical composition of Karak Mudstones, Kohat Plateau, Pakistan; implications for smectite-illitization and provenance. *Sedimentary Geology*, **130**, 229–247.
- Schultz L.G. (1964) Quantitative interpretation of mineralogical composition from X-ray and chemical data for Pierce-Shale. *US Geological Survey Profesional Paper*, 391-C.
- Šucha V., Kraus I., Gerthofferova H., Petes S. & Serekova M. (1993) Smectite to illite conversion in bentonites and shales of the east Slovak basin. *Clay Minerals*, **28**, 243–253.
- Underwood M.B. & Pickering K.T. (1996) Clay-mineral provenance, sediment dispersal patterns, and mud-rock diagenesis in the Nankai accretionary prism, Southwest Japan. *Clays and Clay Minerals*, **44**, 339–356.
- Warr L.N. & Rice A.H.N. (1994) Interlaboratory standardization and calibration of clay mineral crystallinity and crystallite size data. *Journal of Metamorphic Geology*, **12**, 141–152.
- Wiewiora A. & Weiss Z. (1990) Crystallochemical classifications of phyllosilicates based on the unified system of projection of chemical composition: II. The chlorite group. *Clay Minerals*, **25**, 83–92.
- Zane A., Sassi R. & Guidotti C.V. (1998) New data on metamorphic chlorite as a petrogenetic indicator mineral, with special regard to greenschist-facies rocks. *The Canadian Mineralogist*, **36**, 713–726.
- Zhao G., Peacor D.R. & McDowell S.D. (1999) ‘Retrograde diagenesis’ of clay minerals in the Precambrian Freda Sandstone, Wisconsin. *Clays and Clay Minerals*, **47**, 119–130.